DYNA
http://dyna.medellin.unal.edu.co/

UNIVERSIDAD NACIONAL DE COLOMBIA

Effect of the liquid-to-powder ratio on physicochemical properties of calcium phosphate cements and of these properties over Biofilm thickness of adhered Staphylococcus Aureus

Daniel Moreno*, Fabio Vargas & Esperanza López

*Grupo de Investigaciones Pirometalúrgicas y de Materiales GIPIMME, Grupo de Investigación en Materiales y Recubrimientos Cerámicos GIMACYR, Facultad de Ingeniería, Universidad de Antioquia UdeA, Medellín, Colombia. * daniel.morenod@udea.edu.co, fabio.vargas@udea.edu.co, esperanza.lopez@udea.edu.co*

Received: February 22th, 2021. Received in revised form: August 13th, 2021. Accepted: September 22th, 2021.

Abstract
Tricalcium phosphate (TCP) synthetized by high temperature solid state reaction at 1400°C and three derived calcium phosphate cements (CPCs) prepared at liquid to powder (L/P) ratios of 0.33, 0.44 and 0.55 ml/g, respectively, were physicochemically characterized. Calcium deficient hydroxyapatite crystals were identified by scanning electron microscopy on CPC, and differences in crystal sizes were observed at different L/P ratios. Also, the biofilm thickness of two *Staphylococcus Aureus* (*S.aureus*) strains grown for 24 hours on the three CPC are reported. A dependence of the biofilm thickness with the specific surface area (SSA) of CPC was identified. They are directly proportional for non-extracellular polysaccharide substances (EPS) producing *S.aureus* and inversely proportional for EPS producing *S.aureus.* Non-proportional behavior between the SSA and mechanical strength of the CPC was observed as L/P ratio increases.

Keywords: calcium phosphate cement; tricalcium phosphate; *Staphylococcus aureus*; biofilm thickness; specific surface area; Extracellular polysaccharide substances.

Efecto de la relación líquido a polvo en las propiedades fisicoquímicas de cementos de fosfato de calcio y de estos sobre el espesor de Biofilm de Staphylococcus Aureus adherido

Resumen
Se caracterizaron fisicoquímicamente un fosfato tricálcico (FTC) sintetizado por reacción de estado sólido a alta temperatura (1400ºC) y tres cementos de fosfato de calcio (CFC) derivados del FTC con relaciones líquido a polvo (L/P) de 0.33, 0.44 y 0.55 ml/g, respectivamente. Fueron identificados cristales de hidroxiapatita deficiente en calcio por microscopía electrónica de barrido en los CFC y se observaron diferencias en el tamaño de los cristales según la relación L/P. Además, se reporta el espesor de biofilm de dos cepas de *Staphylococcus Aureus* (*S.aureus)* cultivadas por 24 horas en los tres CFC. Se identificó una dependencia del espesor de biofilm con el área superficial específica (ASE) de los CFC: es directamente proporcional si el *S.aureus* no es productor de substancias polisacáridas extracelulares (SPE) e inversamente proporcional si lo es. Se identificó un comportamiento no proporcional entre la ASE y el esfuerzo mecánico de los CFC al incrementar la relación L/P.

Palabras clave: cemento de fosfato de calcio; fosfato tricálcico; *Staphylococcus aureus*; espesor de biofilm; área superficial específica; substancias polisacáridas extracelulares.

1. Introduction

The life expectancy of humans and the world population are continuously increasing in time, giving rise to more abundant people with bone diseases such as osteoporosis, bone cancer, bone fractures, and bone infections [1-3]. As

How to cite: Moreno, D., Vargas, F. and López, E., Effect of the liquid-to-powder ratio on physicochemical properties of calcium phosphate cements and of these properties over Biofilm thickness of adhered Staphylococcus Aureus.. DYNA, 88(219), pp. 102-110, October - December, 2021.

each case may be different, it is necessary for orthopedists to have a broad assortment of materials for a more personalized treatment. Several calcium phosphate (CaP) biomaterials are currently used as bone replacement materials in orthopedic or dentistry surgeries [4-6]. Among them, calcium phosphate cement (CPC) presents interesting characteristics like biocompatibility, osteoconductivity, injectability, *in vivo* self-setting, and the capability to incorporate any kind of active principle (proteins, growth factors, DNA, or drugs). All these characteristics are mainly given by the chemical composition (which is similar to the mineral component of the bone) and by the easy handling of the paste formed when the precursor, alpha tricalcium phosphate (α-TCP), is mixed with an aqueous solution [7-8]. Although CPC is widely used in bone treatment procedures, the research on new CPC formulations is continuously performed.

However, the in vivo behavior of the CPC might be compromised by surgical site infections that lead towards *Osteomyelitis*. Such disease is mainly caused by microorganisms like *Staphylococcus aureus* (*S. aureus*), which adheres to the biomaterial, grows a defined biofilm, and finally promotes an infection that may persist and proliferate to nearby tissues. A biofilm is a 3D structure formed by microorganism aggregates' excretion of extracellular polymer substances (EPS), establishing a safe environment that protects these microorganisms from external chemical components and mechanical stresses [9-12]. One crucial step in the development of a high antibiotic resistant *Osteomyelitis* is the biofilm formation onto the material [13,14]. Thus, it is important to study how thickly and homogenously it grows during the first hours after the implant is colonized by the microorganisms so that future strategies can be proposed for prevention of this phenomena. One recent method for measuring biofilm thickness is by optical coherence tomography (OCT), which is an *in situ*, non-destructive, non-contact characterization technique that enables researchers to obtain a transversal image of the material and the grown biofilm without any contamination of the sample [15,16].

CPC is a biomaterial that can be obtained from TCP; also, CPC is in constant research due to the formation of calcium deficient Hydroxyapatite (CDHA) in a physiological medium, mimicking bone mineral component. Although there are some works that analyze CPC properties' change due to different liquid-to-powder (L/P) ratios [17,18], no surface adhered *S. aureus* biofilm thickness is reported; neither is any relationship between the microorganism thickness and the CPC physicochemical properties reported.

This work aims to analyze the effect of the calcium phosphate cement liquid to powder ratio over its physicochemical properties (microstructure, specific surface area, rugosity, chemical bonds, compression, and flexural strength) and how these are related to the Biofilm thickness of two cement adhered *S. aureus* strains, one EPS producer and the other non-EPS producer.

The understanding of the relation between microorganism and substrate characteristics in the *S. aureus* biofilm formation on calcium phosphate cements would help future works to incorporate new physicochemical strategies to avoid biofilms on ceramics used as bone graft. In addition, the biofilm thickness analysis shown here is a starting point for the efficacy evaluation of CPC loaded with antibacterial agents.

2. Materials and methods

2.1 α-TCP synthesis

α-TCP was synthesized via high temperature solid state reaction by the mixture of calcium carbonate ($CaCO_3$ Merck, Germany) and calcium hydrogen phosphate ($CaHPO_4$ Sigma-Aldrich, USA) at a 2:1 molar ratio. It was prepared with a similar protocol presented by Pastorino *et al* [19], briefly, 16.13 grams of $CaCO_3$ and 43.87 grams of $CaHPO_4$ were mixed in a vertical shaker at 750 RPM. Sequently, the mix was poured into a platinum crucible and heated inside a furnace to 1400ºC, sustained at said temperature for 2 hours, then quenched by air jet and assisted by crushing with a stainless-steel hammer to enhance the powder surface area for cooling. Finally, the α-TCP obtained was milled in a 250 ml zirconia ball mill (S 100 centrifugal ball mill, Retsch GmbH, Germany) using four zirconia balls (d=40 mm) for 25 min at 400 rpm. The α-TCP powder was sieved through a 37 μm hole size mesh (#400 mesh, Pinzuar LTDA, Colombia). To guarantee the α-TCP powder was the desired one, X-ray fluorescence (XRF; Axios WDXRF, PANanlytical B.V., The Netherlands) was used to analyze the chemical composition and to calculate the calcium to phosphorous molar ratio (Ca/P). X-ray diffraction (XRD; Empyrean, PANanalytical B.V., The Netherlands), with a copper radiation source (Cukα, λ = 1.540598 Å), operated at 45 kV and 40 mA was used to determine whether α or β-TCP phases were present on the precursor powder in order to determine the goodness of the thermal process to obtain α-TCP. The XRD pattern was compared with the Joint Committee on Powder Diffraction Standards (JCPDS) 9-348 and 9-169 for the α and β phases, respectively, in the range of 2θ = 20-40º. In addition, Fourier Transformed Infrared Spectrometry (FTIR-DRIFT, IRTracer, Shimadzu, Japan) was developed to ensure the material presented only tricalcium phosphate related ions.

2.2 CPC synthesis

To obtain three different CPCs, α-TCP powder was mixed with distilled water at three different liquid-to-powder ratios (L/P) of 0.33, 0.44, and 0.55 ml/g, noted as C3, C4, and C5, respectively. The agitation of these two components was carried out continuously for one minute prior to molding. Samples for electronic microscopy analysis were poured in Polyethylene cylindrical molds (d=12.0 mm, h=6.0 mm) for compression (d=6.0 mm, h=12.0 mm) and flexural (w=4.0 mm, t=3.0 mm, l=45.0 mm) tests. Teflon molds were used according to ASTM standards C1424 and C1161, respectively. When visual cohesion was achieved, each sample was immersed on Ringer's solution at 37ºC for 7 days to accomplish the setting reactions. Finally, samples were dried at 60ºC for 24 hours and stored in a desiccator. For the analysis of biofilm, formation samples C3, C4, and C5 were poured and molded in a 24 well plate and immersed in Ringer's solution as previously explained. CPC XRD was

obtained with the same characteristics explained for TCP, comparison was made against Hydroxyapatite standard JCPDS 9-432. The SSA was determined by nitrogen (N_2) sorption using a Gemini V2.00 (Micromeritics, USA), and samples for this test were casted as cylinders (d=6.0 mm, h= 4.0 mm) and degassed in a nitrogen atmosphere at 120ºC for 12 h. The SSA analysis is reported using Brunauer–Emmett–Teller (BET) theory. The morphology and homogeneity of the three CPC was analyzed through a scanning electron microscopy (SEM; JSM-6490LV, JEOL Ltd, Japan) to determine whether the formation of calcium deficient Hydroxyapatite (CDHA) crystals was accomplished. Surface roughness was measured by profilometry (Surtronic S100, Taylor Hobson, UK) over the samples for flexural test; measurements were done over the face of the sample that was not in contact to the mold during the process. Both compression and flexural test were performed in a universal testing machine (AGS-X 50 kN, Shimadzu Ltd, Japan) with a head speed of 0.5mm/min.

2.3 S. aureus strains

Two *S. aureus* strains were used in this work: an EPS producing strain (*S. aureus* ATCC 25923) and a non-EPS producing strain (5298 isolated from a patient with an implant-related osteomyelitis at the University Medical Center Groningen, the Netherlands) [20]. Both *S. aureus* strains were thawed from -80ºC to room temperature and incubated on Blood agar plates at 37ºC in anaerobic condition for 24 h. Next, an isolated colony was taken and precultured in 10 ml of tryptone soya broth (TSB; Oxoid Ltd, Basingstoke, England) at 37ºC, anaerobically as well, for 24 h. This preculture was used to prepare a main culture of 100 ml in TSB and incubated for another 16 h at 37ºC.

For the biofilm growth over the CPC, the *S. aureus* main culture was sonicated (3 X 10 s), to break bacterial aggregates, and re-suspended in TSB to a concentration of 5 X 10^8 bacteria/ml, which was guaranteed by using a Bürker-Türk counting chamber. Later, for bacteria incubation, 1.5 ml of this culture was gently deposited over each CPC sample, and as controls, two empty polystyrene (PS) wells were filled, one with the EPS producing and the other with the non-EPS producing strain. The other empty wells were filled with distilled water to guarantee a good humidity level and to avoid culture evaporation. After 2 h, supernatant was replaced by 1.5 ml of fresh TSB, incubated for 16 h at 37ºC, and covered with aluminum foil to prevent liquid from evaporating. The test was performed under static conditions.

2.4 Biofilm analysis

Optical coherence tomography (OCT) images were taken using an OCT GANYMEDE-II (Thorlabs, Germany) at 24 h of incubation. Two images per sample were taken. When running the test, supernatant is replaced by sterile phosphate-buffered saline (PBS) at pH 7.4 for diminishing interference in image acquirement. OCT is an in situ, non-destructive characterization technique [15,16].

The OCT images were processed using open source software imageJ (version 1.51K, National Institute of Health, Bethesda, MD, USA). For biofilm thickness calculation, 10 measurements of each image were carried out. First, the bright bottom line was determined as the CPC surface and the white continuous dots above as the *S. aureus* biofilm. Next, the measurement lines were done from the baseline until the last dot considered present in the biofilm. The lines are perpendicular to the CPC surface at the measuring point. As the three CPC were manually casted in a 24 well plate, no flat cement surface will be observed on OCT images, as it will be seen in PS control.

3. Results and analysis

3.1 Calcium phosphate powder characterization

The XRF analysis of the synthesized calcium phosphate presented a purity of 98.77% as well as a molar Ca/P ratio equal to 1.49, consisting of 53.37±0.21 wt.% of CaCO3 and 44.79±0.30 wt.% of P2O5. The calcium (Ca) and phosphorus (P) elemental composition and the molar Ca/P are presented in Table 1. This result is in accordance with the theoretical molar Ca/P ratio values of 1.5 for tricalcium phosphates [4].

As shown on Fig. 1, the sample XRD diffractogram was compared against the JCPDS 9-348 and 9-169 patterns, and mainly α-TCP peaks were identified in the material diffractogram (Fig. 1). Only one peak at 27.89° was attributed to β-TCP. In accordance to other authors this small impurity may be attributed to small quantities of magnesium, present in the reagents, which stabilizes the β polymorph [21-23] or to a non-fast enough cooling rate, as stated in some documents [24,25]. However, the high α-TCP purity indicates that this precursor will promote an apatite-like calcium phosphate cement if pH during setting is higher than 4.2 [23,26]. These results show that the thermal process used was adequate for obtaining α-TCP.

Table 1.
Tricalcium phosphate elemental chemical composition and Ca/P molar ratio.

	Ca	P	Ca/P
%wt	37.97	19.69	1.93
moles	0.949	0.635	1.49

Source: The authors

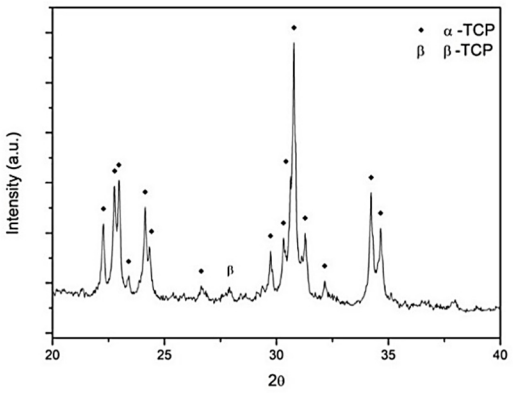

Figure 1. XRD spectra of obtained TCP (Reference: α-TCP JCPDS 9-348, β-TCP JCPDS 9-169).
Source: The authors.

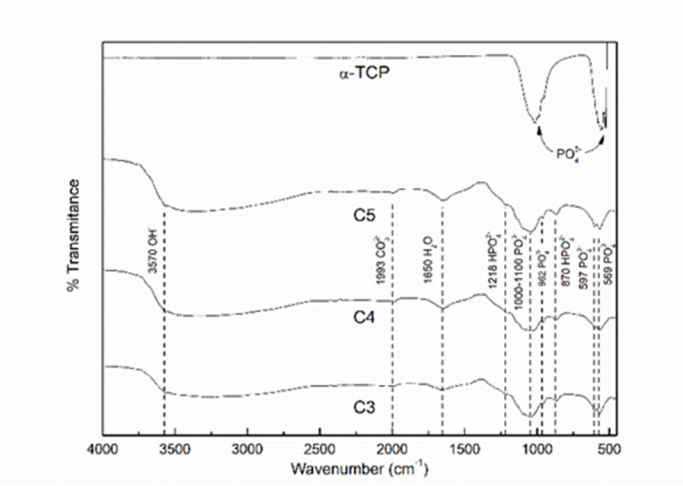

Figure 2. FTIR spectra of α-TCP and 7 days set CPCs at L/P ratios of 0.33 (C3), 0.44 (C4), and 0.55 (C5) ml/g. α-TCP peaks: PO_4^{3-} (526, 556, 955, 989, 1019 cm^{-1}); CPC´s peaks: PO_4^{3-} (569, 590, 962, and 1000-1100 cm^{-1}), HPO_4^{2-} (870 and 1218 cm^{-1}), OH^- (3570 cm^{-1}), H_2O (1650 cm^{-1}), and CO_3^{2-}(1993 cm^{-1}).
Source: The authors.

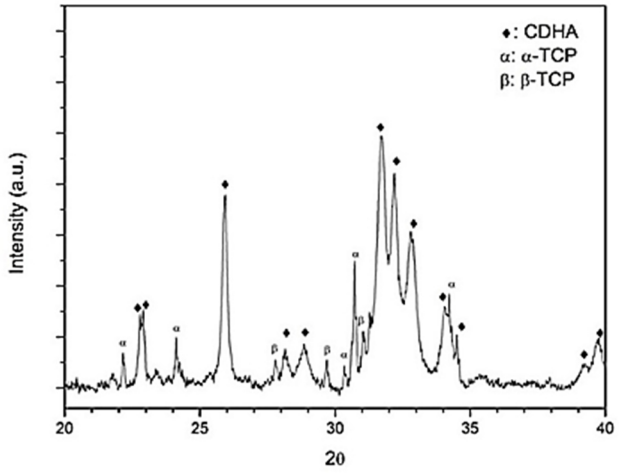

Figure 3. XRD spectra of C4 after setting for 7 days in Ringer's solution (Reference:α-TCP JCPDS 9-348, β-TCP JCPDS 9-169, CDHA JCPDS 9-432).
Source: The authors.

3.2 Calcium phosphate cement characterization

Fig. 2 shows the FTIR spectra of the thermal obtained TCP and of the three CPC. It is possible to see how the α-TCP transforms into the cement after 7 days of setting in Ringer's solution at 37°C. Nevertheless, when comparing the three different L/P ratios cements among them, no difference can be noticed. The α-TCP spectra show two big peaks associated only with phosphate ion (526, 556, 955, 989, 1019 cm^{-1}); on the other hand, C3, C4, and C5 present phosphate related bands (569, 590, 962 and 1000-1100 cm^{-1} band), hydrogen phosphate (870 and 1218 cm^{-1}), hydroxyl (3570 cm^{-1}), and specific peaks showing water (1650 cm^{-1}) and carbonate (1993 cm^{-1}) absorption. The presence of hydroxyl ion indicates that Hydroxyapatite formation has occurred, and the water and carbonate absorption is typical after setting in Ringer's solution due to ions exchange.

The XRD diffractogram of C4, after setting for 7 days, is presented on Fig. 3, where mainly peaks of Calcium deficient Hydroxyapatite (CDHA) is recognized; but some peaks of α-TCP and β–TCP are also observed. This shows that some alpha phase stills remain to react, due to CDHA precipitation on TCP surface which cover these particles, and then the process is then regulated by diffusion of α–TCP through CDHA. As β–TCP is a less reactive phase, after 7 days in Ringer´s solution it is still present on the cement. The morphologies of each CPC after the setting reactions are shown in Fig. 4. Mainly the obtained microstructures shown on micrographs at 5,000X are of crystal aggregates with a fine plate-like structure, which is distinctive of CDHA, or apatite-like cement, derived from α-TCP powder with particle sizes smaller than 37 μm [17,27,28]. The diminishing of the inter-aggregate crystals' size was noted as L/P ratio rose. This phenomenon is due to the major dispersion of α-TCP particles hence creating more nucleation points for the CDHA crystals growth [29,30]. This is also reflected in the micrographs at 500X, as a less dense cement is observed as L/P ratio rises, which is in accordance with other works where CPC porosity was studied as a function of the L/P parameter [18,31].

Maximum compressive and flexural strength are presented on Fig. 5, where both mechanical tests show similar behavior when increasing the L/P ratio. The greater resistance is presented for C4 (11.27 ± 4.02 MPa compression; 7.49 ± 3.71 MPa Flexion) and similar lower values for C3 (8.24 ± 1.88 MPa compression; 4.85 ± 2.98 MPa Flexion) and C5 (5.21 ± 0.36 MPa compression; 3.93 ± 1.26 MPa Flexion). These mechanical results show that there is a non-linear behavior when increasing the L/P ratio in the worked range of 0.33-0.55 ml/g, which may be attributed to moldability differences of the cement pastes when mixing with water at different ratios. C3 is a quiet dry paste that presents discontinuities after molding (also observed on SEM images, Fig. 4a). On the contrary, C5 is a very liquid paste that fills the molds very easily, but it may incorporate air bubbles into the sample, generating large pores that diminish the mechanical strength. C4 has an intermediate moldability which makes it an easy-to-work paste that copies the mold shape well and generates more compact cement which can also be seen on the SEM images, Fig. 4c.

The SSA applying BET theory and surface roughness is reported on Table 2 for each cement condition. It is notorious that the SSA values do not follow a linear behavior, which is inconsistent with what is presented by other researchers [17,32]. In this case, when increasing L/P ratio from 0.33 to 0.44, the SSA diminishes from 16.18 to 13.41 m2 g-1 respectively. However, when L/P ratio is increased towards 0.55, SSA increases as well to 17.18 m2 g-1. This result agrees with the mouldability behavior previously explained where the easier condition for compacting presents the lower SSA (C4) and samples with molding difficulties have higher SSA due to discontinuities and pores. The surface rugosity of samples measured on the face exposed to air is higher for C3, which once again is attributed to the low moldability, but rugosity diminishes to similar values for C4 and C5 which due to their high-water contents allow to give a flatter texture to the samples.

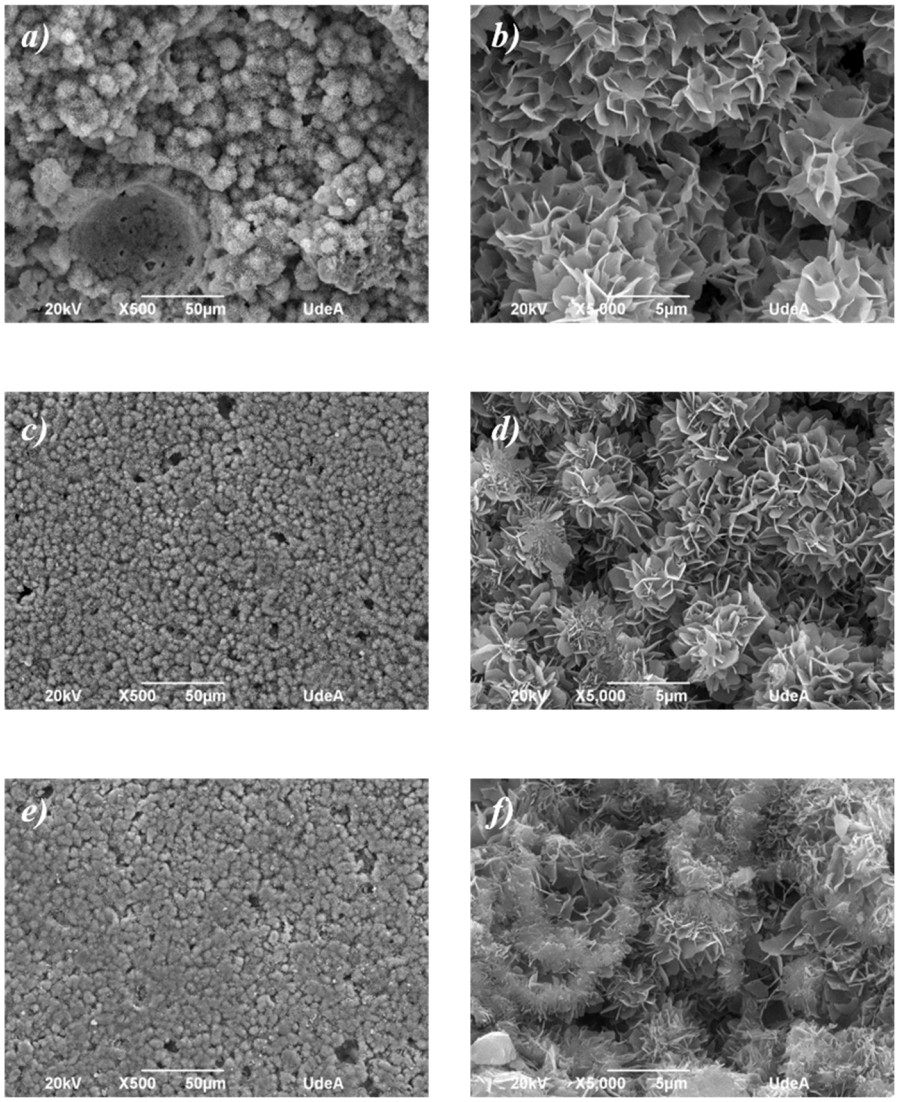

Figure 4. SEM micrographs of the fracture surfaces of the three CPC, C3 *a)* & *b),* C4 *c)* & *d),* and C5 *e)* & *f)*. Scale bars of 50 µm and 5 µm for the images at 500X (left column) and 5000X (right column), respectively.
Source: The authors.

Table 2.
CPC specific surface area (BET theory) and rugosity (Ra).

Cement Condition	L/P ratio	SSA (m2/g)	Ra (µm)
C3	0.33	16.18	4.53
C4	0.44	13.41	1.23
C5	0.55	17.18	1.87

Source: The authors

3.3 Biofilm formation over CPC

The biofilm morphology over the three different CPC can be observed in Fig. 6 after 24 h. of incubation. Although biofilm aggregates may be identified over all samples, the two strains used did not evenly colonize the three CPC surfaces, with exception of ATCC 25923 over C4. However, both biofilm strains grew homogenously on the PS control. On the left side of the image, Fig. 6a shows a mushroom like structure of ATCC 25923 over C3, a distinct structure of biofilms [15,33]. The more stable biofilm is identified for the EPS producing *S. aureus* ATCC 25923 over C4 in Fig. 6c; also, in this biofilm some black areas inside the biofilm are identified, which corresponds to the fact that EPS is a substance that does not disperse the OCT signal; and thus, neither an interference signal nor image is generated.

Overall, the EPS producing *S. aureus* forms a higher biofilm than the non-EPS producing indicating, as reported in other studies [9,34], that EPS gives more stability to these bacteria clusters.

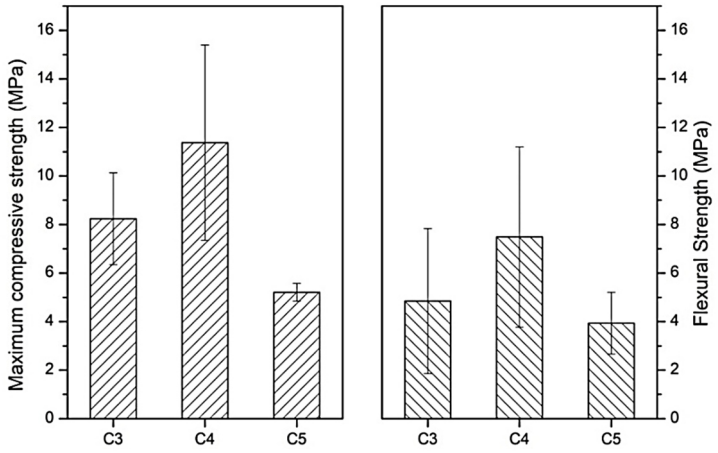

Figure 5. Maximum compressive and flexural strength of the calcium phosphate cements at L/P ratios of C3, C4, and C5 ml/g. Both tests performed at 0.5 mm/min.
Source: The authors.

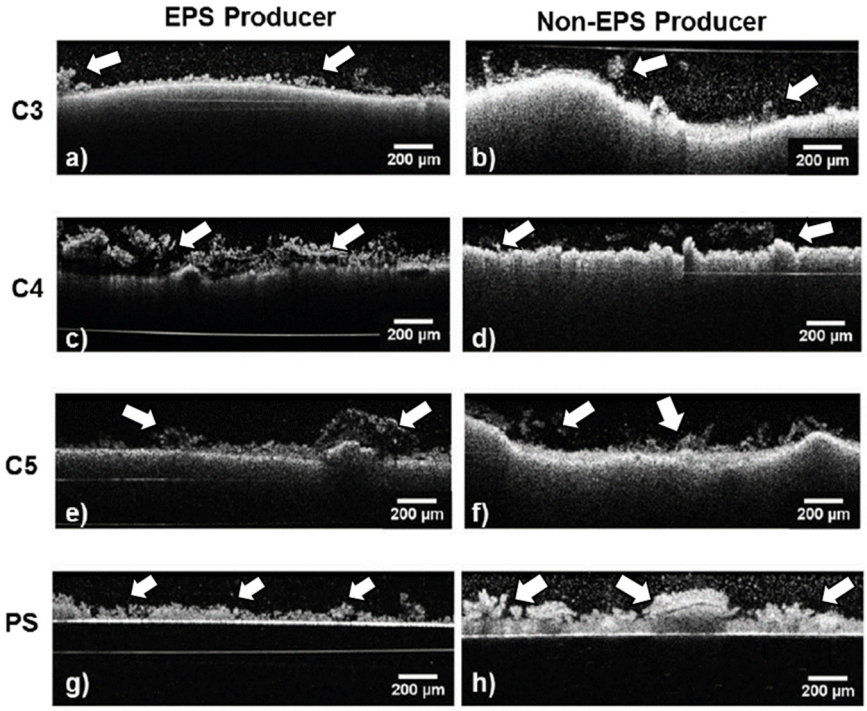

Figure 6. OCT images of the two *S. aureus* strains biofilm after 24h of incubation. ATCC 25923 left column *a),c),e),* and *g)* and 5298 right column *b),d),f),* and *h)* on CPCs (C3 first row; C4 second row; C5 third row) and on PS control (fourth row). Scale bar of 50 µm.
Source: The authors.

Fig. 7 illustrates the biofilm thickness quantification for both EPS and non-EPS producing bacteria (ATCC 25923 and 5298, respectively) after 24 h. of incubation as well as the SSA of the CPC. It is noteworthy that the EPS producing *S. aureus* ATCC 25923 presents the highest biofilm thickness over C4 (258.53 ± 97.73 µm) and the lowest over the C3 (112.92 ± 53.97 µm), being the first greater and the second less than the biofilm thickness over the PS control (179.43 ± 85.20 µm). The opposite behavior is presented by the non-EPS producing *S. aureus* 5298, where the minimum value was obtained on C4 (20.32

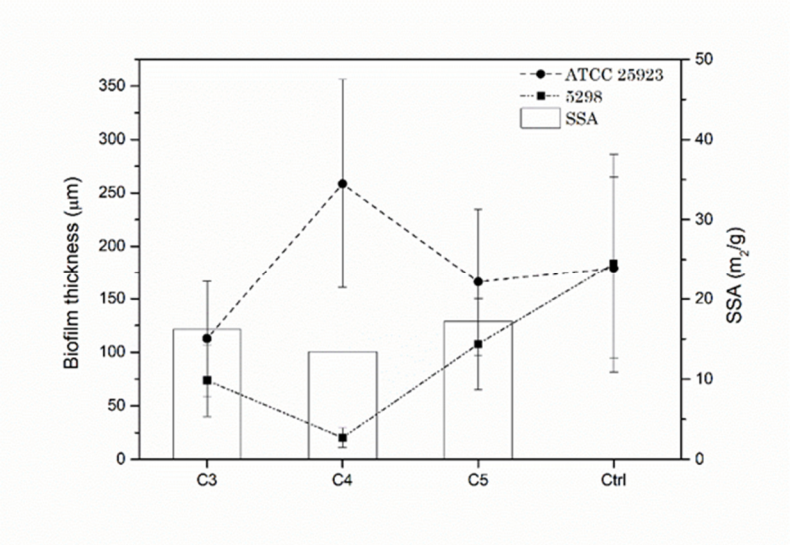

Figure 7. Biofilm thickness quantification of *S. aureus* EPS producing ATCC 25923 (circles) and non-EPS producing 5298 (squares) at 24 h of incubation on CPCs (C3, C4, and C5) and polystyrene empty well control and proportionality against CPCs' SSA (columns). Source: The authors.

± 9.18 µm) and highest over C5 (107.75 ±42.42 µm), all *S. aureus* 5298 biofilm thicknesses were under the PS control value (183.71 ± 52.51 µm; 24h). This indicates that *S. aureus* biofilm thickness behavior is proportional to the CPC SSA for the non-EPS producing bacteria and inversely proportional for the EPS producing one. This may be explained by the fact that the EPS will supply a major surface for the adherence of the bacteria biofilm to the CPC substratum, thus rendering a higher mechanical stability, which is one of the major characteristics of EPS [10,35].

4. Conclusions

The calcium phosphate cement precursor was confirmed to be α-TCP which leads to obtain an apatite-like calcium phosphate cement with fine plate-like aggregate morphology characteristic of CDHA. After 7 days of setting, C3, C4, and C5 present similar characteristics proven by FTIR; however, compression, flexion, SEM, and SSA show non-linear behavior as the L/P ratio was increased, which is attributed to the cement pastes moldability. C4 was easier to manipulate paste and then being the most compact cement with the highest mechanical resistance, indicating that the best tested L/P is 0,44 ml/g in terms of mechanical properties.

Biofilm formation of the Two *S. aureus* strains (the EPS and the non-EPS producing) was confirmed after 24 h of incubation onto the three CPC with L/P ratios of 0.33, 0.44, and 0.55 ml/g. Biofilm thickness showed a behavior with a breaking point above the L/P ratio of 0.44 ml/g (C4). In other words, for the EPS producing bacteria, the biofilm thickness was the highest, while for the non-EPS producing, the thickness was the lowest for this L/P ratio. The SSA of the CPC also showed a non-linear behavior. These two behaviors of the biofilm thickness and the SSA of the CPC suggest that the first is directly proportional to the second in the case of the *S. aureus* 5298 non-EPS producing bacteria. On the contrary, the *S. aureus* ATCC 25923 EPS producing bacteria is inversely proportional. This bacteria slime associated with the EPS not only helps the biofilm to be more resistant to antibiotics and external mechanical stresses but also improves the stability of the bacteria cluster, giving rise to a biofilm that does not depend on the substrate characteristics, such as surface area or porosity. This study has shown that 24 h of incubation of *S. aureus* strains (ATCC 25923 and 5298) is enough time for the growth of a biofilm on any of the three kinds of calcium phosphate cement here tested under static conditions and establish a base for the study of this bacterium over calcium phosphate cements by OCT.

Acknowledgements

This work was financially funded by Colciencias, Colombia (code 1115745-57862, contract 012-2017), the authors present no conflict of interest. We thank professor Dr. Henny C. van der Mei from the department of Biomedical Engineering at the University Medical Center Groningen for providing the S. aureus strains and allowing the use of the optical coherence tomographer.

References

[1] Rennert-May, E., Bush, K., Vickers, D. and Smith, S., Use of a provincial surveillance system to characterize postoperative surgical site infections after primary hip and knee arthroplasty in Alberta, Canada. American Journal of Infection Control,

44(11), pp. 1310-1314, 2016. DOI: 10.1016/j.matchemphys.2008.10.020.
[2] Uskokovic, V., Nanostructured platforms for the sustained and local delivery of antibiotics in the treatment of osteomyelitis. Critical Reviews in Therapeutic Drug Carrier Systems, 32(1), pp. 1-59, 2015. DOI: 10.1615/CritRevTherDrugCarrierSyst.2014010920.
[3] Sadowska, J.M., Genoud, K.J., Kelly, D.J. and O'Brien, F.J., Bone biomaterials for overcoming antimicrobial resistance: Advances in non-antibiotic antimicrobial approaches for regeneration of infected osseous tissue. Materials Today, 46, pp. 136-154, 2021. DOI: 10.1016/j.mattod.2020.12.018.
[4] Dorozhkin, S.V., Calcium orthophosphate bioceramics. Ceramics International, 41, pp. 13913-13966, 2015. DOI: 10.1016/j.ceramint.2015.08.004.
[5] Canillas, M., Pena, P., Aza, A. De. and Rodríguez, M.A., Calcium phosphates for biomedical applications. Boletín de la Sociedad Española de Cerámica y Vidrio, 6, pp. 1-22, 2017. DOI: 10.1016/j.bsecv.2017.05.001.
[6] Mensah, L.M. and Love, B.J., A meta-analysis of bone cement mediated antibiotic release: Overkill, but a viable approach to eradicate osteomyelitis and other infections tied to open procedures. Materials Science and Engineering: C, 123, art. 111999, 2021. DOI: 10.1016/j.msec.2021.111999.
[7] Zhang, J., Liu, W., Schnitzler, V., Tancret, F. and Bouler, J.-M.M., Calcium phosphate cements for bone substitution: Chemistry, handling and mechanical properties. Acta Biomaterialia, 10(3), pp. 1035-1049, 2014. DOI: 10.1016/j.actbio.2013.11.001.
[8] Canal, C. and Ginebra, M.P., Fibre-reinforced calcium phosphate cements: a review. Journal of the Mechanical Behavior of Biomedical Materials, 4(8), pp. 1658-1671, 2011. DOI: 10.1016/j.jmbbm.2011.06.023.
[9] Gusnaniar, N., Sjollema, J., Nuryastuti, T., Peterson, B.W., van de Belt-Gritter, B., de Jong, E.D., et al., Structural changes in S. epidermidis biofilms after transmission between stainless steel surfaces. Biofouling, 33(9), pp. 1-10, 2017. DOI: 10.1080/08927014.2017.1360870.
[10] Billings, N., Birjiniuk, A., Samad, T.S., Doyle, P.S. and Ribbeck, K., Material properties of biofilms—a review of methods for understanding permeability and mechanics. Reports on Progress in Physics, 78(3), art. 036601, 2015. DOI: 10.1088/0034-4885/78/3/036601.
[11] Peterson, B.W., Mei, H.C. van der., Sjollema, J., Busscher, H.J. and Sharma, P.K., A distinguishable role of eDNA in the viscoelastic relaxation of biofilm. MBIO, 4(5), pp. 1-7, 2013. DOI: 10.1128/mBio.00497-13.
[12] Silva, V., Miranda, C., Bezerra, M., Antão, H.S., Guimarães, J., Prada, J., et al., Anti-biofilm activity of dalbavancin against methicillin-resistant Staphylococcus aureus (MRSA) isolated from human bone infection. Journal of Chemotherapy, pp. 1-6, 2021. DOI: 10.1080/1120009X.2021.1911518.
[13] Birt, M.C., Anderson, D.W., Bruce Toby, E. and Wang, J., Osteomyelitis: Recent advances in pathophysiology and therapeutic strategies. Journal of Orthopaedics, 14 (1), pp. 45-52, 2017. DOI: 10.1016/j.jor.2016.10.004.
[14] Furustrand-Tafin, U., Betrisey, B., Bohner, M., Ilchmann, T., Trampuz, A. and Clauss, M., Staphylococcal biofilm formation on the surface of three different calcium phosphate bone grafts: a qualitative and quantitative in vivo analysis. Journal of Materials Science: Materials in Medicine, 26(3), pp. 130, 2015. DOI: 10.1007/s10856-015-5467-6.
[15] Sharma, P., Rozenbaum, R.T., Woudstra, W., de Jong, E.D., van der Mei, H.C., Busscher, H.J., et al., A constant depth film fermenter to grow microbial biofilms. Protocol Exchange, (March), pp 1-21, 2017. DOI: 10.1038/protex.2017.024.
[16] Wagner, M. and Horn, H., Optical coherence tomography in biofilm research: a comprehensive review. Biotechnology and Bioengineering, 114(7), pp. 1386-402, 2017. DOI: 10.1002/bit.26283.
[17] Espanol, M., Perez, R.A., Montufar, E.B., Marichal, C., Sacco, A. and Ginebra, M.P., Intrinsic porosity of calcium phosphate cements and its significance for drug delivery and tissue engineering applications. Acta Biomaterialia, 5(7), pp. 2752-62, 2009. DOI: 10.1016/j.actbio.2009.03.011.
[18] Paknahad, A., Kucko, N.W., Leeuwenburgh, S.C.G. and Sluys, L.J., Experimental and numerical analysis on bending and tensile failure behavior of calcium phosphate cements. Journal of the Mechanical Behavior of Biomedical Materials, 103(November), art 103565, 2020. DOI: 10.1016/j.jmbbm.2019.103565.
[19] Pastorino, D., Canal, C. and Ginebra, M.-P., Drug delivery from injectable calcium phosphate foams by tailoring the macroporosity-drug interaction. Acta Biomaterialia, 12, pp. 250-259, 2015. DOI: 10.1016/j.actbio.2014.10.031.
[20] Rasyid, H.N., Van Der Mei, H.C., Frijlink, H.W., Soegijoko, S., van Horn, J.R., Busscher, H.J., et al., Concepts for increasing gentamicin release from handmade bone cement beads. Acta Orthopaedica, 80(5), pp. 508-513, 2009. DOI: 10.3109/17453670903389782.
[21] Carrodeguas, R.G., De Aza, A.H., Turrillas, X., Pena, P. and De Aza, S., New approach to the β→α polymorphic transformation in magnesium-substituted tricalcium phosphate and its practical implications. Journal of the American Ceramic Society, 91(4), pp. 1281-1286, 2008. DOI: 10.1111/j.1551-2916.2008.02294.x.
[22] García-Páez, I.H., Carrodeguas, R.G., De Aza, A.H., Baudín, C. and Pena, P., Effect of Mg and Si co-substitution on microstructure and strength of tricalcium phosphate ceramics. Journal of the Mechanical Behavior of Biomedical Materials, 30C, pp. 1-15, 2013. DOI: 10.1016/j.jmbbm.2013.10.011.
[23] Torres, P.M.C.C., Abrantes, J.C.C.C., Kaushal, A., Pina, S., Döbelin, N., Bohner, M., et al., Influence of Mg-doping, calcium pyrophosphate impurities and cooling rate on the allotropic α↔β-tricalcium phosphate phase transformations. Journal of the European Ceramic Society, 36(3), pp. 817-827, 2016. DOI: 10.1016/j.jeurceramsoc.2015.09.037.
[24] O'Hara, R., Buchanan, F. and Dunne, N., Injectable calcium phosphate cements for spinal bone repair. Biomaterials for Bone Regeneration, Elsevier, 2014, pp. 26-61.
[25] Loca, D., Sokolova, M., Locs, J., Smirnova, A. and Irbe, Z., Calcium phosphate bone cements for local vancomycin delivery. Materials Science and Engineering: C, 49, pp. 106-13, 2015. DOI: 10.1016/j.msec.2014.12.075.
[26] Montufar, E.B., Maazouz, Y. and Ginebra, M.P., Relevance of the setting reaction to the injectability of tricalcium phosphate pastes. Acta Biomaterialia, 9(4), pp. 6188-6198, 2013. DOI: 10.1016/j.actbio.2012.11.028.
[27] Ginebra, M.P., Driessens, F.C.M. and Planell, J.A., Effect of the particle size on the micro and nanostructural features of a calcium phosphate cement: a kinetic analysis. Biomaterials, 25(17), pp. 3453-62, 2004. DOI: 10.1016/j.biomaterials.2003.10.049.
[28] O'Neill, R., McCarthy, H.O., Montufar, E.B., Ginebra, M.P., Wilson, D.I., Lennon, A., et al., Critical review: injectability of calcium phosphate pastes and cements. Acta Biomaterialia, 50, pp. 1-19, 2017. DOI: 10.1016/j.actbio.2016.11.019.
[29] Chen, W.-C., Lin, J.-H.C. and Ju, C.-P., Transmission electron microscopic study on setting mechanism of tetracalcium phosphate/dicalcium phosphate anhydrous-based calcium phosphate cement. Journal of Biomedical Materials Research. Part A, 64, pp. 664-671, 2003. DOI: 10.1002/jbm.a.10250.
[30] Li, J., Xu, W., Lin, X., Cao, F., Yang, J., Li, L., et al., A Ca-deficient a-deficient hydroxyapatite (CDHA)/MgF_2 bi-layer coating with unique nano-scale topography on biodegradable high-purity Mg. Colloids and Surfaces B: Biointerfaces, 190(November), art. 110911, 2020. DOI: 10.1016/j.colsurfb.2020.110911.
[31] Pastorino, D., Canal, C. and Ginebra, M.-P., Multiple characterization study on porosity and pore structure of

calcium phosphate cements. Acta Biomaterialia, 28, pp. 205-214, 2015. DOI: 10.1016/j.actbio.2015.09.017.
[32] Canal, C., Pastorino, D., Mestres, G., Schuler, P. and Ginebra, M.P., Relevance of microstructure for the early antibiotic release of fresh and pre-set calcium phosphate cements. Acta Biomaterialia, 9(9), pp. 8403-8412, 2013. DOI: 10.1016/j.actbio.2013.05.016.
[33] Burtseva, O., Baulina, O., Zaytseva, A., Fedorenko, T., Chekanov, K. and Lobakova, E., In vitro biofilm formation by bioluminescent bacteria isolated from the marine fish Gut. Microbial Ecology, 81(4), pp. 932-940, 2021. DOI: 10.1007/s00248-020-01652-0.
[34] Gusnaniar, N., Sjollema, J., Jong, E.D., Woudstra, W., de Vries, J., Nuryastuti, T., et al., Influence of biofilm lubricity on shear-induced transmission of staphylococcal biofilms from stainless steel to silicone rubber. Microbial Biotechnology, 10(6), pp. 1744-1752, 2017. DOI: 10.1111/1751-7915.12798.
[35] Ren, Z., Kim, D., Paula, A.J., Hwang, G., Liu, Y., Li, J., et al., Dual-targeting approach degrades biofilm matrix and enhances bacterial killing. Journal of Dental Research, 98(3), pp. 322-330, 2019. DOI: 10.1177/0022034518818480.

D. Moreno, received a BSc. Eng. in Materials Engineering in 2012 from University of Antioquia, a MSc. in Advanced Materials Engineering in 2015 from Polytechnic University of Catalonia, Spain, and a PhD in Materials Engineering in 2019 from University of Antioquia, Colombia. His research is emphasized in polymeric, metallic, and ceramic biomaterial development and in surface functionalization to avoid bacteria adhesion. At the moment, he is an assistant professor at the Faculty of Engineering of the University of Antioquia.
ORCID: 0000-0002-9088-3112.

F. Vargas, in the first five years of his professional experience, he participated in research projects developing new materials for the oil industry in Colombia. in 2013 he began his career as auxiliary professor in the Department of Materials Engineering at the Universidad de Antioquia, Colombia, where he is currently full professor. His research is focused on ceramic coatings manufactured by thermal spraying processes; he has published more than 30 scientific papers, half of them in journals ranked as Q1. He is co-author of 1 patent and 2 trade secrets. He has been awarded with: primer puesto en las II Jornadas de Innovación Tecnológica en Ecopetrol, Maestro de Ingenieros, Universidad de Antioquia y Thèse Très Honorable de la Universidad de Limoges. Currently is ranked as senior researcher for Colciencias.
ORCID: 0000-0003-4484-3950.

E. López, is BSc. in Mining and Metallurgical Engineer in 1991 from the Universidad Nacional de Colombia, the MSc. in Metallurgical Engineering in 1999 from the Santander Industrial University, Colombia and the PhD in Science and Technology of Materials in 2006 from the Oviedo University, Spain. Her research is emphasized in ceramic materials, advanced ceramics, biomaterials, nanostructured materials, ceramic coatings, materials recycling, extractive metallurgy. At the moment, she is a professor at the Faculty of Engineering of University of Antioquia.
ORCID: 0000-0002-1038-6504.